# Kinetics of Hydrogen Radical Reactions with Toluene Including Chemical Activation Theory Employing System-Specific Quantum RRK Theory Calibrated by Variational Transition State Theory

Junwei Lucas Bao, Jingjing Zheng, and Donald G. Truhlar*

Department of Chemistry, Chemical Theory Center, and Supercomputing Institute, University of Minnesota, Minneapolis, Minnesota 55455-0431, United States

S *Supporting Information*

ABSTRACT: Pressure-dependent reactions are ubiquitous in combustion and atmospheric chemistry. We employ a new calibration procedure for quantum Rice—Ramsperger—Kassel (QRRK) unimolecular rate theory within a chemical activation mechanism to calculate the pressure-falloff effect of a radical association with an aromatic ring. The new theoretical framework is applied to the reaction of H with toluene, which is a prototypical reaction in the combustion chemistry of aromatic hydrocarbons present in most fuels. Both the hydrogen abstraction reactions and the hydrogen addition reactions are calculated. Our system-specific (SS) QRRK approach is adjusted with SS parameters to agree with multistructural canonical variational transition state theory with multidimensional tunneling (MS-CVT/SCT) at the high-pressure limit. The new method avoids the need for the usual empirical estimations of the QRRK parameters, and it eliminates the need for variational transition state theory calculations as a function of energy, although in this first application we do validate the falloff curves by comparing SS-QRRK results without tunneling to multistructural microcanonical variational transition state theory (MS-μVT) rate constants without tunneling. At low temperatures, the two approaches agree well with each other, but at high temperatures, SS-QRRK tends to overestimate falloff slightly. We also show that the variational effect is important in computing the energy-resolved rate constants. Multiple-structure anharmonicity, torsional—potential anharmonicity, and high-frequency-mode vibrational anharmonicity are all included in the rate computations, and torsional anharmonicity effects on the density of states are investigated. Branching fractions, which are both temperature- and pressure-dependent (and for which only limited data is available from experiment), are predicted as a function of pressure.
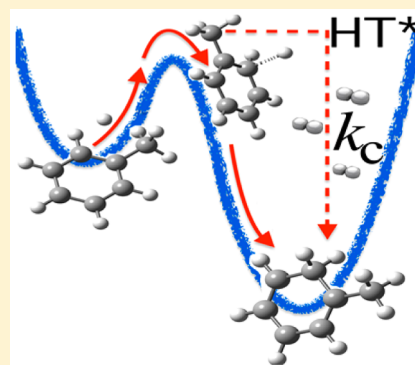
1. INTRODUCTION

Aromatic compounds with 7—10 carbon atoms constitute about 34% of commercial gasoline.[1] Adding toluene or other alkyl aromatics to gasoline increases the octane rating,[2] which indicates the performance of an internal combustion engine fuel, and the higher the value, the more compression the fuel can withstand before ignition. Toluene is the simplest alkylbenzene and is a prime candidate for detailed study to understand the combustion of alkylbenzenes. Toluene is also widely used as an organic solvent, precursor, or feedstock in synthesis and industry.

The reaction of hydrogen atoms with toluene is one of the important elementary reactions in the combustion of toluene and is the subject of this article. The reactions we are considering in the present study are shown in Scheme 1. There are three classes of reactions in this scheme: hydrogen abstraction (R1—R4), hydrogen addition followed by stabilization of an intermediate (R5—R8), and hydrogen addition followed by decomposition of an intermediate to form benzene (R9). In this paper, we refer to reactions R5—R8, i.e., methylcyclohexadienyl production reactions, as "addition reactions" and reaction R9, which is a two-step substitution reaction in which the first step is an addition, as "formation of benzene" (denoted as k_{benzene}). The abstracted

hydrogen can be from the methyl group or the ortho, meta, or para position of the benzene ring, and the addition rate is also site-dependent. Robb et al.[3] measured the overall rate constant of H + toluene using the heterogeneous removal of atomic hydrogen on molybdenum oxide. Sauer and Ward[4] reported the rate constant for producing methylcyclohexadienyl radical (the sum of the rate constants for reactions R5—R8) at total pressures of 12 and 61 atm (mainly Ar) at 298 K. Using gas chromatography, Robaugh and Tsang[5] measured the ratio of the sum of rate constants for R1—R4 to the rate constant for H + CH$_4$ → H$_2$ + CH$_3$ at 950—1100 K and 2—5 atm of Ar, and they also measured the ratio of rate constant for R9 to this methane rate constant over the same temperature and pressure range. Hippler and co-workers[6] measured the rate constant of R1 from 600—1800 K using shock waves and pyrolysis of C$_2$H$_5$I as H atom source. Ellis et al.[7] determined the rate constants for reactions R1 and R9 at 773 K and 500 Torr of a mixture of H$_2$, N$_2$, and O$_2$ as bath gas. (The amount of each gas varies in different runs.) Hanson et al.[8] measured the rate constant of R1 from 1256 to

Scheme 1. Reactions of Hydrogen Atoms with Toluene[a]
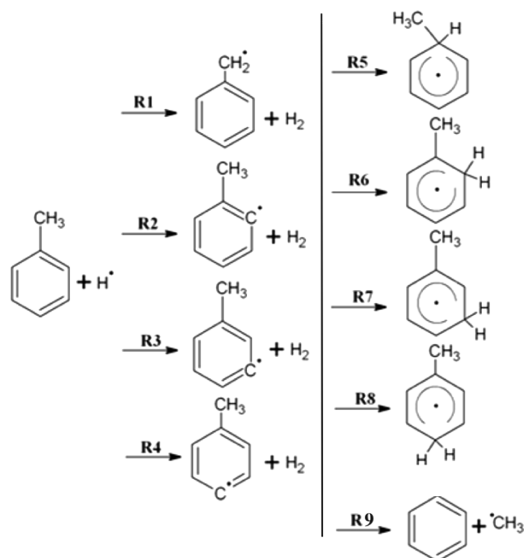
[a]Hydrogen abstraction (R1−R4), hydrogen addition followed by stabilization of an intermediate (R5−R8), and hydrogen addition followed by decomposition of an intermediate to form benzene (R9).

1667 K at 1.7 bar of Ar by using UV laser absorption of benzyl radicals in high-temperature shock-tube experiments.

There are two components to any dynamical calculation. The first is the calculation or modeling of structures, energies, and vibrational frequencies; the second is the calculation of dynamics per se. An important approach in modern computational kinetics is the use of direct dynamics in which instead of using a predefined potential energy function or empirical thermochemical data about reactants and empirical thermochemical kinetics data about transition states "...all required energies and forces for each geometry that is important for evaluating dynamical properties are obtained directly from electronic structure calculations."[9] The present work employs this approach for both unimolecular and bimolecular processes. For the dynamical step, the theory for bimolecular reactions[10] is much more advanced than the theory for unimolecular reactions, and one of the objectives of the present study is to advance the latter theory as introduced next.

Abstraction reactions such as R1−R4 are bimolecular reactions in both the forward and reverse direction; because it is generally safe to consider such reactions at the high-pressure-limit, the pressure effects on these rate constants are not discussed for these reactions. The chemical activation theory, i.e., the main new development of the present paper, is applied only to adducts formed in association reactions, which are unimolecular reactions in the reverse direction; for such reactions, nonequilibrium effects are very important, which is the motivation for the new theory presented here. There are two kinds of pressure-dependent nonequilibrium effects in gas-phase kinetics. The first is "falloff," which is characterized by the depletion of the more reactive (higher-energy) states of a thermally activated reactant when the pressure is not high enough to repopulate them faster than they react; in this case, a unimolecular reaction rate falls off as the pressure decreases. The unimolecular rate constants are smaller than the equilibrium high-pressure ones. The second effect, which is the subject of this work, involves the decomposition of a newly formed adduct. If stabilizing collisions are not effective enough to produce a thermal distribution of

internal states of the adduct prior to its reaction, then the adduct is said to be chemically activated, and it reacts from a nonequilibrium distribution of states, yielding a unimolecular rate constant larger than the high-pressure equilibrium one. In contrast, the rate constants for the reverse association reactions of unimolecular decompositions are lowered as the pressure is lowered from the high-pressure limit. For association reactions (such as the present addition reactions), this is due to the possibility of redissociation before energy transfer collisions thermally stabilize the nascent adducts. The effect can be very large because the usual experimental pressures are far from high-pressure-limit for unimolecular reactions. In the Lindemann−Hinshelwood theory for unimolecular dissociation reactions (covered in most kinetics textbooks), the pressure-dependent rate constants reduce to the high-pressure equilibrium limit when the collisional energy transfer rate is significantly higher than rate of the dissociation process; at lower pressures, the rate of reaction is equal to the second-order reaction rate of collisional activation, which is proportional to the concentration of bath gas. The proper way to treat such effects is by a master equation;[10−13] however, in the present work we use a simpler method that requires much less input data. In particular, the pressure-dependent rate constants for hydrogen addition reactions (R5−R8) are treated in terms of a chemical activation mechanism. Pressure dependence of unimolecular rate constants is a standard topic in chemical kinetic texts, but despite its importance, such effects in current practice are often treated with empirical estimation of frequency factors and activation energies, as in the original version of the very useful and widely used quantum Rice−Ramsperger−Kassel (QRRK) formalism of Dean.[14] It is important to develop less empirical methods that nevertheless retain the simplicity necessary for building mechanisms and reaction networks.

The present work provides a methodology that eliminates the empirical estimation of frequency factors and activation energies of the previous QRRK method but retains its simplicity as needed for wide application in combustion mechanisms and for convenient interpretation of experimental results. In particular, high-pressure multistructural canonical variational theory[15−17] (MS-CVT) rate constants are used to calibrate QRRK rate constants. The resulting method, called system-specific QRRK or SS-QRRK, combines a chemical activation mechanism,[18,19] QRRK theory,[14,20,21] MS-CVT, and Troe's modified strong collision assumption[22−24] for the rate of energy transfer. This approach can provide reasonable estimates of pressure effects in an efficient way, and the use of QRRK theory eliminates the need for employing multistructural microcanonical variational theory (MS-μVT), although in the present work we do verify the new methodology by comparing results obtained with SS-QRRK theory to more complete calculations employing MS-μVT.

As examples of chemical activation effects in combustion systems, Lefort and Tsang[25] presented an empirically based approach to deriving the pressure-dependent rate constants of chemically activated reactions of adducts formed by association of methyl radicals with aromatic radicals. They used a hindered rotor model but noted that they "...do not attach any particular physical significance to the hindrance...", rather it is used to "...calibrate an empirical methodology..." with a special emphasis on applicability of their approach to large molecules.

The present work considers the chemically activated reactions of adducts formed by association of hydrogen atoms with toluene, and we also place a special emphasis on making the calculations more affordable for large molecules, in our case by

developing the (SS)-QRRK theory that incorporates the modified strong-collision method in chemical activation theory to provide an efficient and nonempirical method for predicting pressure-dependent rate constants of unimolecular reactions based on direct dynamics calculations of the high-pressure rate constant. Furthermore, the present work also develops MS-μVT, which is a more rigorous way to compute the microcanonical rate constants and compares results thus obtained with our SS-QRRK theory to judge the quality of the theory. Thus, we attempt to advance the theory in two ways: (i) at the high-pressure-limit in which we use MS-CVT/small-curvature tunneling approximation theory (SCT)[34] with modern exchange-correlation density functionals for electronic structure calculations and (ii) in the intermediate- and low-pressure regimes for which we developed SS-QRRK. Note that MS-CVT/SCT is applicable for both bimolecular and unimolecular processes, and it has been widely used in previous work for abstraction reactions[26−28] and high-pressure unimolecular isomerizations.[29,30] However, at the usual experimental pressures, chemical activation effects are especially important for R5−R9, and theories taking account of these effects are developed and utilized here for the first time.

In the work reported here, we carried out first-principles direct dynamics calculations using MS-CVT[15−17,31,32] to calculate the pressure-independent rate constants of reactions R1−R4, and we used MS-CVT and MS-μVT[33] in a chemical activation formalism to calculate the pressure-dependent rate constants of reactions R5−R8. All MS-CVT calculations include tunneling by the SCT[34] and anharmonicity by methods introduced in the second to last paragraph of this introduction. It will be shown that our computational results are consistent with experimental observations.

For reactions R6−R8, we consider the following mechanism:

$$ H + T \underset{k_{-1}(E)}{\overset{k_1(T)}{\rightleftharpoons}} HT^* \xrightarrow{k_c[M]} HT $$
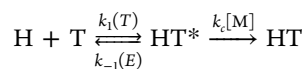
where T is still temperature, T is toluene, H is the hydrogen atom, HT is the addition product (methylcyclohexadienyl radical), HT* is the energized adduct, and M is the bath gas, which is H_2 in the present work. The rate constants k_1 of the formation of HT* via addition reactions are the high-pressure-limit rate constants, which are considered to be functions of temperature and are therefore computed in a canonical ensemble by MS-VTST. The dissociation rate constants $k_{-1}(E)$ are treated as functions of total energy, where we make the RRK assumption that the dissociation rate constant depends only on total energy. The collisional deactivation rate constants are denoted as k_c. The rate constant of formation of the stabilized HT adduct is called k_{stab}, which is defined as $(d[HT]/dt)/([H][T])$, where brackets denote a concentration in molecules per unit volume.

For reaction R5, the following mechanism is used, which allows two possible dissociation processes of HT*:

$$ H + T \underset{k_{-1}(E)}{\overset{k_1(T)}{\rightleftharpoons}} HT^* \xrightarrow{k_2(E)} C_6H_6 + CH_3 $$
$$ \downarrow k_c[M] $$
$$ HT $$
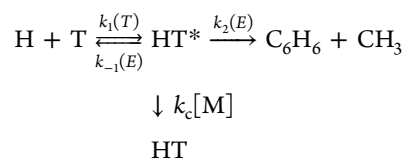
where $k_2(E)$ is the energy-dependent unimolecular dissociation rate constant of the energized species HT*. The rate constant of formation of the stabilized HT adduct is again k_{stab}. Breaking the carbon−carbon bond in HT* leads to the formation of benzene and methyl radical (reaction R9′); we call the rate constant of the

formation of benzene $k_{benzene}$, which is defined as $(d[C_6H_6]/dt)/([H][T])$.

Vibrational anharmonicity effects, which include torsional anharmonicity and high-frequency-mode anharmonicity, play an important role in the kinetics of many chemical reactions.[26,28,35−40] Torsional anharmonicity has two components, i.e., multiple-structure anharmonicity and torsional potential anharmonicity, and they are included here by the multistructural torsion (MS-T) method,[41−44] which includes the contributions from all the distinguishable conformers of the reactants and the transition states. At very low temperature (where $k_B T \ll \hbar\omega$), low-frequency modes can often be treated well enough with the harmonic-oscillator approximation; at the high-temperature limit (where $k_B T$ is much higher than the torsional barrier), internal rotation can be computed by a free-rotor model. In the middle range of temperature, torsions have to be treated explicitly, and we treat torsional modes on the basis of an approximated reference fully coupled torsional partition function in the MS-T method, in which only the Hessians of local minima are required. The MS-T partition function is a summation of the rovibrational partition functions of all the distinguishable conformers with the corresponding Boltzmann weight. We also investigated the torsional anharmonicity effects on the density of states for one of the transition states of the toluene + H reactions.

Note that zero-point energy (ZPE) is usually dominated by high frequencies. High-frequency-mode anharmonicity is often included by scaling the normal force constants or frequencies with an empirical scaling factor. Frequency-scaling factors are usually smaller than unity, which means that partition functions are increased by using a frequency-scaling factor. It is often true that anharmonicity of a stretching mode increases the partition function; however, anharmonicity of a bend mode could either increase or decrease the partition function. To take anharmonicity into account in more detail, one can use different scale factors for bends and stretches,[45] but in the present work, we use a singe scale factor[46] for a given structure. We test the validity of this method by using vibrational perturbation theory.[47−50]

In section 2.1, we explain the calculation of the high-pressure-limit rate constants. In section 2.2, we explain how we calculate k_{stab} and $k_{benzene}$ in terms of elementary rate constants k_1, k_{-1}, k_2, and k_c of the above pressure-dependent mechanisms. In section 2.3, we explain how we calculated these elementary rate constants. Readers who are interested in the results and discussion but not the theoretical methodology and computational details can skip sections 2 and 3 and go directly to section 4.

2. THEORETICAL METHODOLOGIES

2.1. High-Pressure-Limit Rate Constants: Unimolecular and Bimolecular. In the present study, toluene and all of the transition state structures have only one torsional degree of freedom, which is the internal rotation of the methyl group. The torsion of a methyl group generates indistinguishable structures and thus does not contribute multiple-structure anharmonicity, but it does contribute torsional potential anharmonicity, which has a local periodicity of 3. Technically speaking, there is a second torsion in one of the cases: In particular, the transition state for abstracting H from the methyl group is phenyl−methylene−H−H, and there is a torsion around the methylene−H bond because the C−H−H bond angle is not exactly 180°. However, this bond angle for the optimized geometry is 179.1°, and therefore C−H−H is treated as a linear bend[51] rather than as a torsion.

(Unphysical results would be obtained by treating it as a nondegenerate bend with an additional torsion.)

Although torsional anharmonicity does not contribute multiple-structure anharmonicity in any of the reactions, the transition states for R6 and R7 have nonsuperimposable mirror images, so these transition states have multiple (two) structures. Thus, all reactions except R6 and R7 could be treated by single-structure variational transition state theory. (Even R6 and R7 could be treated in this way because when the multiple-structure anharmonicity is due entirely to an optically active transition state it can be treated by symmetry numbers.)[52] Nevertheless, single-structure CVT/SCT is a special case of MS-CVT/SCT, and the multiple-structure version provides a convenient way to treat torsional potential anharmonicity. Therefore we apply MS-CVT/SCT to all the cases.

The MS-CVT/SCT high-pressure-limit rate constants for the thermal rate constants of reactions R1−R8 at temperature T are given by

$$k^{\text{MS-CVT/SCT}} = \kappa^{\text{SCT}} \frac{k_{\text{B}} T}{h} \frac{Q_{\text{con−ro−vib}}^{\text{CVT-MS-T}}}{\Phi^{\text{R-MS-T}}} e^{-V_{\text{MEP}}(s=s_*^{\text{CVT}})/k_{\text{B}}T} \tag{1}$$

for the bimolecular reactions and by

$$k^{\text{MS-CVT/SCT}} = \kappa^{\text{SCT}} \frac{k_{\text{B}} T}{h} \frac{Q_{\text{con−rovib}}^{\text{CVT-MS-T}}}{Q_{\text{con−rovib}}^{\text{R-MS-T}}} e^{-V_{\text{MEP}}(s=s_*^{\text{CVT}})/k_{\text{B}}T} \tag{2}$$

for the unimolecular reactions, which in the present case are dissociation reactions, where k_{B} is Boltzmann's constant, h is Planck's constant, κ^{SCT} is the SCT transmission coefficient, $V_{\text{MEP}}(s = s_*^{\text{CVT}})$ is the potential energy relative to reactants along the minimum-energy path (MEP) evaluated with the reaction coordinate s equal to its value at the canonical variational transition state, $Q_{\text{con−rovib}}^{\text{CVT-MS-T}}$ is the conformational−rotational−vibrational partition function (with zero of energy at $V_{\text{MEP}}(s = s_*^{\text{CVT}})$) of the canonical variational generalized transition state (GT) evaluated by the MS-T method, $Q_{\text{con−rovib}}^{\text{R-MS-T}}$ is the conformational−rotational−vibrational partition function of the reactant evaluated by MS-T method, and $\Phi^{\text{R−MS-T}}$ is the reactant partition function per unit volume computed by the MS-T method as

$$\Phi^{\text{R-MS-T}} = Q_{\text{rot−vib}}^{\text{toluene-MS-T}} Q_{\text{ele}}^{\text{toluene}} Q_{\text{ele}}^{\text{H}} \left[\frac{2\pi m_{\text{toluene}} m_{\text{H}} k_{\text{B}} T}{(m_{\text{toluene}} + m_{\text{H}})h^2} \right]^{3/2} \tag{3}$$

where $Q_{\text{rot−vib}}^{\text{toluene−MS-T}}$ is the rotational−vibrational partition function of toluene with torsional potential anharmonicity.

The electronic partition functions of all the species, $Q_{\text{ele}}^{\text{X}}$ (X = GT, toluene, and H), are assumed to be equal to the degeneracy of the ground state, which for the present reactions is 2 for an odd number of electrons and 1 for an even number of electrons.

Although some reactions have two transition state structures, as discussed above, those structures are optical isomers. Therefore, we need to calculate only one MEP per reaction. The canonical variational transition state is determined by variationally optimizing (in a canonical ensemble) the position of the dividing surface as a function of distance s along the MEP while including torsional anharmonicity as a function of s. (This may be called full MS-VTST,[33] as opposed to the original MS-VTST,[15] in which torsional anharmonicity effects were evaluated only at the stationary points.)

The high-pressure rate constants are fitted by the following equations:[53,54]

$$k = \begin{cases} A\left(\dfrac{T}{300}\right)^n \exp\left[-\dfrac{E(T + T_0)}{R(T^2 + T_0^2)}\right] & \text{endothermic reaction} \\[3mm] A\left(\dfrac{T + T_0}{300}\right)^n \exp\left[-\dfrac{E(T + T_0)}{R(T^2 + T_0^2)}\right] & \text{exothermic reaction} \end{cases} \tag{4}$$

The temperature-dependent Arrhenius activation energy E_a (which is also called the Tolman activation energy)[55,56] is defined by

$$E_a(T) = -R \, \text{d}(\ln k) / \, \text{d}(1/T) \tag{5}$$

which yields

$$k(T) = A(T) \exp[-E_a(T) / RT] \tag{6}$$

and

$$E_a = \begin{cases} \dfrac{E(T^4 + 2T_0 T^3 - T_0^2 T^2)}{(T^2 + T_0^2)^2} + nRT & \text{endothermic reaction} \\[3mm] \dfrac{E(T^4 + 2T_0 T^3 - T_0^2 T^2)}{(T^2 + T_0^2)^2} + \dfrac{nRT^2}{T + T_0} & \text{exothermic reaction} \end{cases} \tag{7}$$

2.2. Observable Pressure-Dependent Rate Constants.
In this section, we explain how the stabilization rate constant k_{stab} and the benzene formation rate constant k_{benzene} are calculated in terms of elementary rate constants.

2.2.1. Observable Pressure-Dependent Rate Constants by Quantum RRK Theory. Applying the steady-state approximation to the chemical activation mechanism yields[14,18]

$$k_{\text{stab}} = k_1^{\text{MS-CVT/SCT}} \sum_{E_0}^{+\infty} \frac{k_c[\text{M}] f(E)}{k_c[\text{M}] + k_{-1}^{\text{QRRK}}(E) + k_2^{\text{QRRK}}(E)} \tag{8}$$

$$k_{\text{benzene}} = k_1^{\text{MS-CVT/SCT}} \sum_{E_0}^{+\infty} \frac{k_2^{\text{QRRK}}(E) f(E)}{k_c[\text{M}] + k_{-1}^{\text{QRRK}}(E) + k_2^{\text{QRRK}}(E)} \tag{9}$$

for reaction R5 and

$$k_{\text{stab}} = k_1^{\text{MS-CVT/SCT}} \sum_{E_0}^{+\infty} \frac{k_c[\text{M}] f(E)}{k_c[\text{M}] + k_{-1}^{\text{QRRK}}(E)} \tag{10}$$

for reactions R6−R8, where $f(E)$ is the fraction of energized species (HT*) at energy E, which is given by

$$f(E) = \frac{k_{-1}^{\text{QRRK}}(E) \, K(E)}{\sum_{E_0}^{+\infty} k_{-1}^{\text{QRRK}}(E) \, K(E)} \tag{11}$$

where

$$K(E) = \exp\left(\frac{-nh\nu}{k_{\text{B}}T}\right) \left[1 - \exp\left(\frac{-h\nu}{k_{\text{B}}T}\right)\right]^s \frac{(n + s - 1)!}{n!(s - 1)!} \tag{12}$$

In eqs 8−10, [M] is the concentration of the bath gas, which is calculated using the ideal gas law, $[\text{M}] = p/RT$, E_0 is the critical energy for reaction, which in SS-QRRK theory is set to be equal to $E_a(T)$ determined from MS-CVT/SCT high-pressure-limit rate constants and may also be called the threshold energy, and QRRK denotes quantum RRK theory or SS-QRRK theory.

The summations in eqs 8−11 are evaluated with a step size of one quantum ($h\overline{\nu}$).

2.2.2. Observable Pressure-Dependent Rate Constants by MS-μVT. If, instead of using QRRK theory in the chemical activation mechanism, we use MS-μVT, then the rate constants of the previous subsection are replaced by the following. For reaction R5, we have

$$k_{stab} = k_1^{MS\text{-}CVT/SCT}$$
$$\int_{E_0}^{+\infty} \frac{k_c[M]\, g(E)}{k_c[M] + k_{-1}^{MS\text{-}\mu VT}(E) + k_2^{MS\text{-}\mu VT}(E)}\, dE \tag{13}$$

$$k_{benzene} = k_1^{MS\text{-}CVT/SCT} \int_{E_0}^{+\infty} \frac{k_2^{MS\text{-}\mu VT}(E)\, g(E)}{k_c[M] + k_{-1}^{MS\text{-}\mu VT}(E) + k_2^{MS\text{-}\mu VT}(E)}\, dE \tag{14}$$

where $g(E)$ is defined as[18]

$$g(E) = \frac{k_{-1}^{MS-\mu VT}(E)\, \rho_R^{MS\text{-}T}(E)\, \exp(-E/k_B T)}{\int_{E_0}^{+\infty} k_{-1}^{MS\text{-}\mu VT}(E)\, \rho_R^{MS\text{-}T}(E)\, \exp(-E/k_B T)\, dE} \tag{15}$$

and for reactions R6−R8 we have

$$k_{stab} = k_1^{MS\text{-}CVT/SCT} \int_{E_0}^{+\infty} \frac{k_c[M]\, g(E)}{k_c[M] + k_{-1}^{MS\text{-}\mu VT}(E)}\, dE \tag{16}$$

In eqs 13−16, $k_{-1}^{MS\text{-}\mu VT}(E)$ and $k_2^{MS\text{-}\mu VT}(E)$ are MS-μVT rate constants, E_0 is barrier height including zero-point vibrational energies in MS-μVT theory, and $\rho_R^{MS\text{-}T}(E)$ is the density of states of the adduct HT computed from MS-T conformational−rovibrational partition functions.

2.3. Pressure Dependence for Reactions R5−R9. *2.3.1. Dissociation Rate Constants.* As indicated in section 2.2, the energy-dependent rate constants in this work are computed by one of two methods: (1) QRRK theory, which will be calibrated to MS-CVT/SCT, or (2) MS-μVT.

2.3.1.1. Quantum RRK Method for Dissociation Rate Constant. Despite its simplicity, QRRK theory has been shown capable of predicting the falloff effects with reasonable accuracy;[14,20,57] $k^{QRRK}(E)$ is computed as the rate constant for a quantum mechanical oscillator with an energy E, with s degenerate modes of frequency $\overline{\nu}$ and with a frequency A of intramolecular energy exchange to accumulate an energy E_0 in a single mode. This yields[21,58]

$$k^{QRRK}(E) = A \frac{n!\,(n - m + s - 1)!}{(n - m)!\,(n + s - 1)!} \tag{17}$$

where n is the number of quanta excited at energy E ($n = E/h\overline{\nu}$), m is the number of quanta at the threshold energy E_0 ($m = E_0/h\overline{\nu}$), and s is the number of vibrational degrees of freedom for the energized complex computed as $3N - 6$ for nonlinear species where N is the number of atoms (for HT*, $s = 42$). The factorial $x!$ is computed by using the gamma function $x! = \Gamma(x + 1)$ for $x <$ 168 or by Stirling's approximation, $x! = \sqrt{2\pi}\, x^{x+1/2} \exp(-x + 1/12x)$, for $x \geq 168$.

Our treatment does not involve dividing the actual number of modes by 2, as is done in many older empirical treatments; we note that it has been shown that choosing s equal to the number of vibrational degrees of freedom (without dividing by 2) can satisfactorily reproduce the experimental falloff curve for

recombination of CH_3 radicals.[14] We also show in this work that using s equal to $3N - 6$ can generate a $k(E)$ curve in the medium-energy range that is in good agreement with the one computed by MS-μVT. (See the Results and Discussion section.)

Schranz and co-workers also proposed modified QRRK theories called 2s-QRRK and QRRK$_\omega$ theory, which can be more accurate than the single-frequency QRRK approach for reproducing the RRKM falloff curve,[59] and Bozzelli, Dean, and co-workers[60−63] developed a three-frequency version. Although these theories can be expected to be more realistic than the original single-frequency version, they need more effort for obtaining the parameters involved, so the present work uses the simple and efficient original method of Dean but with less empiricism. Thus, we neither abandon QRRK theory nor complicate it with multiple frequencies; rather, we show how it can be modified in its single-frequency form to be accurate while remaining very practical, as we demonstrate in this work. Our SS-QRRK theory maintains the simplicity of the original single-frequency version while incorporating the accuracy of state-of-the-art multistructural variational transition state theory with the small-curvature tunneling approximation in order to explicitly include variational effects, tunneling, multiple structures, and torsional potential anharmonicity.

Because vibrational frequencies in real molecules are not degenerate, we compute $\overline{\nu}$ as the geometric mean vibrational frequency for the stabilized adduct HT, which is computed as

$$\overline{\nu} = (\prod_{i=1}^{s} \nu_i)^{1/s} \tag{18}$$

Notice that, in the classical limit, where $n - m \gg s$, quantum RRK theory reduces to classical RRK theory:

$$k(E) = A \left(\frac{E - E_0}{E} \right)^{s-1} \tag{19}$$

We show eq 19 here in order to make a connection between QRRK theory and classical RRK theory; however, we do not apply classical RRK theory in this work for computing microcanonical rate constants.

Integrating the QRRK rate constant $k^{QRRK}(E)$ in the canonical ensemble yields $k(T)$ in Arrhenius form.[18] Thus, to practically apply the QRRK theory, the high-pressure limit of the Arrhenius pre-exponential factor and activation energy are used for A and E_0.[18] The way that this is done is the major difference between the present treatment and that of Dean. Dean used empirical relations for these parameters, and we determine them from direct dynamics MS-CVT/SCT calculations.

The MS-CVT/SCT calculations are described in section 2.1. Here we describe their use to calibrate the QRRK formula. First, MS-CVT/SCT high-pressure-limit rate constants are computed and then fitted using eq 4; activation energies are calculated by eq 7. The critical energy of QRRK theory is set equal to the MS-CVT/SCT activation energy

$$E_0(T) = E_a(T) \tag{20}$$

and the frequency factor A in QRRK theory is set equal to the Arrhenius pre-exponential factor of eq 6, which yields

$$A(T) = k^{MS\text{-}CVT/SCT}(T) \exp[E_a(T)/RT] \tag{21}$$

Notice that in such an approach multistructural torsional effects, variational effects, and tunneling have been approximately included in the obtained SS-QRRK microcanonical rate

constants; A does not need to be estimated empirically as in the previous[14] work.

Note that E_a and E_0 are different quantities, but E_0 is interpreted differently depending on the context. In particular, E_0 is the effective barrier height or threshold energy in MS-μVT, whereas E_0 is a phenomenological parameter or effective threshold energy in the SS-QRRK method proposed here. In the SS-QRRK treatment, E_0 is determined by fitting the most accurate available high-pressure-limiting $k(T)$, which includes multifrequency, MS-T, variational, and SCT effects. We use E_a from the high-pressure limit rather than that from a computed barrier height as the effective threshold energy in SS-QRRK because when you integrate QRRK over a canonical ensemble you get eq 6 with constant A and E_a. One should not interpret the SS-QRRK effective threshold energy of the present treatment as an actual barrier or threshold energy on the potential energy surface.

2.3.1.2. Variational Transition State Theory for Dissociation Rate Constant. The elementary rate constants $k_{-1}(E)$ and $k_2(E)$ can also be computed using MS-μVT. The MS-μVT rate constant $k^{\text{MS-}\mu\text{VT}}(E)$ is

$$k^{\text{MS-}\mu\text{VT}}(E) = \Gamma^{\mu\text{VT}}(E)\, k^{\text{MS-TST}}(E) \qquad (22)$$

where $\Gamma^{\mu\text{VT}}(E)$ is the microcanonical variational transmission coefficient and $k^{\text{MS-TST}}(E)$ is the microcanonical conventional transition state theory rate constant[64−67] with multistructural anharmonicity:[33]

$$k^{\text{MS-TST}}(E) = \frac{N_{\text{TS}}^{\text{MS-T}}(E)}{h\, \rho_{\text{R}}^{\text{MS-T}}(E)} = \frac{N_{\text{GT}}^{\text{MS-T}}(E,\, s=0)}{h\, \rho_{\text{R}}^{\text{MS-T}}(E)} \qquad (23)$$

where $N_{\text{TS}}^{\text{MS-T}}(E)$, $\rho_{\text{R}}^{\text{MS-T}}(E)$, and $N_{\text{GT}}^{\text{MS-T}}(E, s)$ are, respectively, the sum of states (SOS) of the conventional transition state, the density of states (DOS) of the reactant (adduct HT), and the SOS of the generalized transition state at location s. The DOS is computed by the inverse Laplace transform[73] (IL) of the MS-T partition function using the steepest-descents method. Integrating DOS from zero to a given rovibrational energy E yields the sum of states at energy E.

The microcanonical variational transmission coefficient is determined by minimizing the sum of states along the reaction coordinate s:

$$\Gamma^{\mu\text{VT}}(E) = \frac{\min_{s} N_{\text{GT}}^{\text{MS-T}}(E,\, s)}{N_{\text{GT}}^{\text{MS-T}}(E,\, s=0)} \qquad (24)$$

where $N_{\text{GT}}^{\text{MS-T}}(E, s)$ is calculated from the IL of the conformational−rotational−vibrational partition function along the reaction coordinate s; $\Gamma^{\mu\text{VT}}(E)$ can deviate significantly from unity and can be a strong function of energy. Integrating $k^{\text{MS-}\mu\text{VT}}(E)$ with the population (probability distribution) of the reactant (adduct) over energy gives the $k^{\text{MS-}\mu\text{VT}}(T)$:

$$k^{\text{MS-}\mu\text{VT}}(T) = \frac{1}{Q_{\text{con−rovib}}^{\text{R-MS-T}}} \int_{0}^{+\infty} k^{\text{MS-}\mu\text{VT}}(E)\, \rho_{\text{R}}^{\text{MS-T}}(E)\, e^{-E/k_{\text{B}}T}\, \mathrm{d}E \qquad (25)$$

It is useful to define V_a^{AG} as the maximum along the reaction coordinate s of the ground-state vibrationally adiabatic potential curve (where this curve is defined as the sum of the potential energy and the local ZPE along the MEP) and to define

$$\Delta V_a^{\text{AG}} = V_a^{\text{AG}} - \varepsilon_{\text{R}}^{\text{G}} \qquad (26)$$

where $\varepsilon_{\text{R}}^{\text{G}}$ is the ZPE of the reactant, with both V_a^{AG} and $\varepsilon_{\text{R}}^{\text{G}}$ measured relative to the overall zero of energy at the reactant equilibrium structure. Because $k^{\text{MS-}\mu\text{VT}}(E)$ is zero for $E < V_a^{\text{AG}}$, only the populations of reactant with energy higher than the vibrationally adiabatic ground-state barrier contribute to the integral. In the present study, we find that microcanonical variational thermal rate constants $k^{\text{MS-}\mu\text{VT}}(T)$ are very close to the canonical variational thermal rate constants $k^{\text{MS-CVT}}(T)$ (Results and Discussion).

To include tunneling in energy-dependent rate constants, we generalize the canonical ground-state tunneling approxima-tion[17,68] that we have used successfully for thermal rate constants with both CVT and μVT[33] thermal rate constants. To include tunneling for thermal μVT rate constants, we used

$$k^{\text{MS-}\mu\text{VT/SCT}}(T) = \kappa^{\text{SCT}}(T)\, k^{\text{MS-}\mu\text{VT}}(T) \qquad (27)$$

To include tunneling for energy-dependent rate constants, we can replace eq 24 with

$$\gamma^{\mu\text{VT/SCT}}(E) = \frac{N^{\text{MS-}\mu\text{VT/SCT}}(E)}{N_{\text{GT}}^{\text{MS-T}}(E,\, s=0)} \qquad (28)$$

The essence of this approximation is to use the tunneling and nonclassical reflection probabilities for the ground-state vibra-tionally adiabatic potential curve for all passage through all the quantized energy levels. Let the ground-state tunneling probability be $P^{\text{SCT}}(E)$, and note that it satisfies

$$P^{\text{SCT}}(E) = \begin{cases} P^{\text{SCT}}(E) & E \le V_a^{\text{AG}} \\ [1 - P^{\text{SCT}}(2V_a^{\text{AG}} - E)] & V_a^{\text{AG}} < E \le V_a^{\text{AG}} + \Delta V_a^{\text{AG}} \\ 1 & E > 2V_a^{\text{AG}} - \varepsilon_{\text{R}}^{\text{G}} \end{cases} \qquad (29)$$

Also note that

$$N^{\text{MS-}\mu\text{VT}}(E) = \sum_{n=0} \theta[E - V_a^{A}(n, s^*(E))] \qquad (30)$$

where θ is a Heaviside step function, $s^*(E)$ is the location of the microcanonical variational transition state at energy E, and

$$V_a^{A}(n, s) = V_{\text{MEP}}(s) + \varepsilon(n, s) \qquad (31)$$

where $\varepsilon(n, s)$ is the local vibrational energy of state n at location s along the MEP. Note that the sum over n goes over all states of all conformations of the transition state, $n = 0$ is the ground state, and the sum continues up in energy until it converges or until one reaches the dissociation energy of the transition state. The microcanonical ground-state tunneling approximation then involves replacing $N^{\text{MS-}\mu\text{VT}}(E)$ by

$$N^{\text{MS-}\mu\text{VT/SCT}}(E) = \sum_{n=0} P^{\text{SCT}}[E + V_a^{A}(0, s^*(E)) - V_a^{A}(n, s^*(E))] \qquad (32)$$

This can be rewritten as a convolution of the tunneling probability with the density of states, but we shall not use $N^{\text{MS-}\mu\text{VT/SCT}}(E)$ in the calculations of this paper.

2.3.2. Collisional Deactivation Rate Constants. The colli-sional deactivation rate constants k_c are computed using Troe's modified strong-collision model,[23,24] which is a simplification that eliminates the need to solve the master equation. Dean and co-workers[69,70] compared the pressure falloff predicted by solving the master equation to that predicted using Troe's modified strong-collision model; they found generally similar results and pointed out that the differences are often smaller than

the uncertainties because of not knowing the appropriate values of the energy transfer parameters.[70] The modified strong-collision model assumes that k_c is the rate constant for collisions sufficiently strong to cause deactivation of energized molecules and that it is given by the product of a collision efficiency β_c and a Lennard-Jones collision rate constant k_{LJ};[24] the collision efficiency factor accounts for the fact that not all the collisions lead to deactivation. For strong collisions, $\beta_c = 1$; for very weak collisions, $\beta_c \ll 1$.

The collision efficiency is computed by solving the following equation:[22-24]

$$\frac{\beta_c}{1 - \beta_c^{1/2}} = \frac{|\langle \Delta E \rangle|}{F_E k_B T} \tag{33}$$

where $\langle \Delta E \rangle$ is the average vibrational energy transferred during both energization and de-energization processes. (Note that $|\langle \Delta E \rangle|$ is smaller than the often-encountered $\langle \Delta E \rangle_{down}$ parameter that is the average energy transferred in collisions in which the vibrational energy goes down.) F_E is the thermal fraction of unimolecular states above the threshold energy and is defined in Troe's work.[23] For moderate-sized molecules, F_E is nearly unity.[22] The temperature dependence of F_E can be treated with Troe's method when it is needed.[23]

The Lennard-Jones collision rate constant k_{LJ} is the product of the hard-sphere collision rate constant[18] k_{HS} and the dimensionless reduced collision integral $\Omega_{2,2}^*$, which is defined by Hirschfelder et al.[71] Therefore

$$k_c = \beta_c \Omega_{2,2}^* k_{HS} \tag{34}$$

The values of the reduced collision integral can be evaluated by numerical integration and have been fitted by other workers with various simple algebraic expressions.[23,24,72,73] In the present study, we choose Troe's fitting expression[23,24] for computing $\Omega_{2,2}^*$:

$$\Omega_{2,2}^* = \begin{cases} \left[0.697 + 0.5185 \log_{10}\left(\frac{k_B T}{\varepsilon_{A-M}} \right) \right]^{-1} & \frac{k_B T}{\varepsilon_{A-M}} \in [3, 300] \\ \left[0.636 + 0.567 \log_{10}\left(\frac{k_B T}{\varepsilon_{A-M}} \right) \right]^{-1} & \frac{k_B T}{\varepsilon_{A-M}} \notin [3, 300] \end{cases} \tag{35}$$

where ε_{A-M} is the Lennard-Jones interaction parameter between molecule A and M and is computed as the geometric average of ε_{A-A} and ε_{M-M}.

The hard-sphere collision rate constant k_{HS} is computed as

$$k_{HS} = \pi \left(\frac{d_A + d_M}{2} \right)^2 \sqrt{\frac{8 k_B T}{\pi \mu}} \tag{36}$$

where the vdW diameters d_A and d_M are computed from the Lennard-Jones parameters σ_{A-A} and σ_{M-M} using the relation $d = 2^{1/6}\sigma$ and μ is the reduced mass of A and M.

3. COMPUTATIONAL DETAILS

3.1. Electronic Structure Calculations and Direct Dynamics. The CVT and μVT calculations were performed via direct dynamics by MPW1K[85]/MG3S[86] using Gaussrate[74] and Polyrate[75] software packages; MS-T partition functions are computed using MSTor software.[76] The SCT approximation was used for tunneling calculations. Electronic structure calculations are carried out with Gaussian 09[77] and the locally modified version.[78] Computational details of the electronic structure and direct dynamics calculations are given in the Supporting Information.

3.2. Deactivating Collisions. In the current work, we choose $|\langle \Delta E \rangle| = 92$ cm^{-1} as determined by Hippler's experimental work[79] on toluene colliding with bath gas H$_2$, and we choose $|\langle \Delta E \rangle| = 130$ cm^{-1} on toluene colliding with bath gas Ar.[79] We choose $F_E = 1.15$, which is the value previously adopted in treating the collisional activation/deactivation processes for radical addition to unsaturated hydrocarbons,[14] such as the CH$_3$ + C$_2$H$_2$ and H + benzene systems.

The Lennard-Jones parameters, ε/k_B and σ, that we used are 410 K and 6.0 Å for HT (taken to be the same as that for toluene),[80] 38 K and 2.93 Å for H$_2$,[72] and 120 K and 3.4 Å for Ar.[81]

All the reported pressure-dependent rate constants are based on H$_2$ gas as the bath gas. (Sauer and Ward,[4] in their experiments at 298 K, used a mixture of H$_2$ and Ar as bath gas, but changing the bath gas to Ar does not make any noticeable difference for falloff effects at 298 K because the falloff effect at 298 K is negligible for either third body.)

4. RESULTS AND DISCUSSION

4.1. Selection of Electronic Structure Method. We tested a large number of electronic structure methods, especially multilevel methods and combinations of exchange-correlation functions with a variety of basis sets. (Please refer to the Supporting Information for detailed discussions.) By comparison to results calculated with the relatively accurate CCSD(T)-F12a[82,83]/jun-cc-pVTZ[84] method, we selected MPW1K[85]/MG3S[86] as the affordable electronic structure method with the best accuracy for reactions R1–R8.

4.2. Applicability of Universal Scaling Factor for Vibrational Anharmonicity. In the calculations of the vibrational frequencies and ZPEs, there are two potential sources of error in conventional treatments: One is the error from the electronic structure calculations, i.e., the electronic structure method we use (wave function theory or density functional theory) is not capable of generating accurate potential energy surface because of the inexactness of the treatment of electron exchange and correlation; the other one arises from adoption of the harmonic-oscillator approximation, which truncates the series expansion of the potential energy at the second-order terms. This section is concerned with correcting the harmonic approximation.

Our treatment of anharmonicity combines two strategies: (1) We account for the dominant anharmonicity in torsions, which are essentially always low-frequency modes, by the MS-T method that in general accounts for both multiple-structure anharmonicity and torsional potential anharmonicity. (See section 4.1 above.) This is particularly important at high temperature, and we have discussed torsional anharmonicity in the previous section. (2) We account for the dominant anharmonicity in other modes by a universal scaling factor for the frequencies. This is particularly important for calculating the ZPE and low-temperature enthalpies because the high-frequency modes that dominate the ZPE are not torsions. The present section is concerned with strategy 2 and testing its applicability for the present reaction.

To make the computed values close to the experimental values, the scaling factors for reproducing the experimental harmonic frequencies, fundamental frequencies, and ZPEs are developed on the basis of a database that consists of 15 small molecules for which the experimental values are available. For a given model chemistry, a single (universal) scaling factor is used to scale all the vibrational frequencies in order to reproduce the experimental vibrational ZPEs. In the dynamics calculations, one often uses the so-developed scaling factor to scale all the computed frequencies for reproducing accurate ZPEs. A previous study[36] has pointed out that such approach may not be reliable for some systems in

Table 1. Harmonic Vibrational Zero-Point Energies and Anharmonic Vibrational Zero-Point Energies (kcal/mol) Computed by HDCPVT2 Method at MPW1K/MG3S Level

	toluene	TS1	TS2	TS3	TS4	TS5	TS6	TS7	TS8
ZPE(harmonic)[a]	82.26	80.77	80.89	80.78	80.80	83.57	83.23	83.17	83.18
ZPE(anharmonic)[b]	81.31	79.55	79.81	79.62	79.75	82.54	82.18	82.12	82.11
λ^{Anh}[c]	0.988	0.985	0.987	0.986	0.987	0.988	0.987	0.987	0.987
λ^{ZPE}[d]	0.958	0.954	0.956	0.955	0.956	0.957	0.957	0.957	0.956

[a]ZPEs are computed using harmonic-oscillator approximation without using any scaling factor. [b]ZPEs are computed based on HDCPVT2 theory, in which the vibrational anharmonicity has been taken into account. [c]λ^{Anh} represents the correction solely for vibrational anharmonicity at a given model chemistry; λ^{Anh}= ZPE(anharmonic)/ZPE(harmonic) [d]λ^{ZPE} is the scaling factor for improving the accuracy of computed ZPE, which corrects both vibrational anharmonicity and accuracy of electronic structure method; $\lambda^{\text{ZPE}} = \lambda^{\text{Anh}}\lambda^{\text{H}}$, where λ^{H} only corrects the accuracy of electronic structure method. We considered its value as the same for all species ($\lambda^{\text{H}} = 0.969$ for MPW1K/MG3S).

Table 2. MS-T Anharmonicity Factors for Forward (fwd) and Reverse (rev) Reactions R1−R8[a]

	R1		R2		R3		R4		R5		R6		R7		R8	
T (K)	fwd	rev	fwd	rev	fwd	rev	fwd	rev	fwd	rev	fwd	rev	fwd	rev	fwd	rev
300	2.51	0.97	1.44	1.04	0.87	1.50	0.98	1.04	2.81	3.30	5.26	2.03	3.20	6.79	1.52	0.59
400	2.91	0.99	1.46	1.04	0.87	1.49	0.98	1.04	3.28	3.38	5.63	1.90	3.26	6.07	1.54	0.52
600	3.65	1.02	1.48	1.04	0.86	1.49	0.98	1.04	4.00	3.41	6.08	1.70	3.31	5.11	1.55	0.43
1000	4.91	1.05	1.51	1.04	0.87	1.48	0.98	1.04	4.90	3.23	6.52	1.41	3.38	4.02	1.57	0.34
1500	6.02	1.03	1.52	1.03	0.86	1.48	0.98	1.05	5.48	2.93	6.76	1.18	3.40	3.28	1.58	0.28
2400	7.28	0.95	1.53	1.03	0.87	1.49	0.98	1.04	6.03	2.47	6.94	0.93	3.43	2.53	1.59	0.21

[a]All results in this table are calculated by MPW1K/MG3S. A table with more temperatures is given as Table S12.

which the anharmonicity effects for the reactants and the transition states are not similar, i.e., different scaling factors have to be utilized for reactants and transition structures in order to describe the vibrational anharmonicity as accurately as possible.

A scaling factor (denoted as λ^{ZPE}) for improving the accuracy of computed ZPEs can be rewritten as a product of two factors: One factor is the scaling factor (denoted as λ^{Anh}) for solely correcting vibrational anharmonicity with a given electronic structure theory, and this scaling factor is in principle molecule- and structure-specific. (However, in practice, we usually use a universal scaling factor.) Another factor (denoted as λ^{H}) is the scaling factor for correcting the errors that solely come from the chosen electronic structure theory, and the value of this scaling factor is considered to be the same for all the molecules and structures.

To test the applicability of the universal scaling factor of the ZPEs to scale all the computed harmonic vibrational frequencies for all the species involved in the current work, we computed the vibrational frequencies and the ZPEs using the hybrid[47] degeneracy-corrected[48] second-order perturbation theory (HDCPT2)[49,50] for treating the vibrational anharmonicity. The molecule-specific anharmonicity factors λ^{Anh}, which solely represent the correction to the vibrational anharmonicity at a given model chemistry, are computed as the ratio of HDCPT2 anharmonic ZPE to the computed harmonic ZPE (without using scaling factor); the universal scaling factor for the harmonic frequencies at a given model chemistry, λ^{H}, is determined as the ratio of computed harmonic frequencies to experimentally extrapolated harmonic frequencies and therefore only represents the correction to the electronic structure method (for MPW1K/MG3S, $\lambda^{\text{H}} = 0.969$). The molecule- and structure-specific scaling factor for ZPE, λ^{ZPE}, is determined by multiplying λ^{H} with λ^{Anh}.

Computed results are shown in Table 1. As we can see from Table 1, the anharmonicity factors λ^{Anh} of various species involved in toluene + H reactions are very close. The standard deviation for λ^{Anh} is 0.0011, which means that the anharmonicity corrections for all the species in the current work are essentially

the same. The average value for λ^{ZPE} is 0.956, which happens to be equal to the universal scaling factor for ZPE at MPW1K/MG3S level. Therefore, for the reactions investigated in the present work, we concluded that using the universal scaling factor for correcting the vibrational anharmonicity is adequate.

Therefore, a universal scaling factor 0.956 was used to scale all the normal-mode and generalized-normal-mode frequencies in all calculations reported here.[46]

4.3. Multiple-Structure and Torsional Anharmonicity. The rotation of the methyl group does not contribute to multistructural anharmonicity, whereas the nonsuperimposable mirror images do. In general, the torsional anharmonicity consists of multiple-structure anharmonicity and torsional potential anharmonicity. All of the local minima involved in reactions R1−R8 have one conformer, the transition structures (TSs) of reactions R1−R4, R5, and R8 have one conformer, and those of reactions R6 and R7 have two conformers (one pair of enantiomers). Thus, the multiple-structure anharmonicity contributes either 1 or 2, and the rest of the torsional anharmonicity is due to torsional potential anharmonicity.

The multiple-structure and torsional anharmonicity effects on MS-CVT rate constants are characterized by the torsional anharmonicity $F_{\text{act}}^{\text{MS-T}}$ factor, which is defined as follows:

$$F_{\text{act}}^{\text{MS-T}} = \frac{Q_{\text{TS}}^{\text{MS-T}}/Q_{\text{TS}}^{\text{SS-HO}}}{Q_{\text{R}}^{\text{MS-T}}/Q_{\text{R}}^{\text{SS-HO}}} \tag{37}$$

where TS stands for the transition state and R stands for reactant (toluene). The calculated $F_{\text{act}}^{\text{MS-T}}$ factors for both forward and reverse reactions are listed in Table 2, which shows that the torsional anharmonicity is quite significant, contributing factors as small as 0.2 and as large as 7.3 to the calculated reaction rates.

The computed quasi-harmonic vibrational frequency of the torsional degree of freedom for toluene molecule is 23.84 cm^{-1}. This very low frequency mode causes great torsional potential anharmonicity; therefore, the partition function decreases greatly. The ratio of the single-structure torsional rovibrational

(SS-T) partition function to single-structure quasi-harmonic rovibrational (SS-QH) partition is 0.463 at 200 K, 0.246 at 800 K, and 0.144 at 2400 K. We also increase the integration grid to "superfine" (150 radial shells around each atom and 974 angular points in each shell) to reoptimize and compute frequencies for toluene to make sure that this low-frequency mode is not due to the insufficiency of the integration grid; at superfine grid, the frequency of this torsional mode is 23.99 cm^{-1}, which means that our choice of integration grid (99 radial shells around each atom and 974 angular points in each shell) is sufficient.

For TS6, the quasi-harmonic vibrational frequency of the torsional degree of freedom is 85.36 cm^{-1}, which is much higher than the one in the toluene molecule. The ratio of SS-T to SS-QH partition function is 1.07 at 200 K, 0.78 at 800 K, and 0.50 at 2400 K.

The DOS and SOS are needed for computing microcanonical rate constants by MS-μVT. Table 3 lists the DOS and SOS of

Table 3. Density of States and Sum of States for TS6 by Inverse Laplace Transform[a]

E (kcal/mol)	DOS (eV^{-1}) MS-QH(IL)	DOS (eV^{-1}) MS-T(IL)	SOS MS-QH(IL)	SOS MS-T(IL)
0.01	2.05×10^6	2.05×10^6	5.92×10^2	5.92×10^2
1.00	1.12×10^8	1.35×10^8	1.52×10^6	1.82×10^6
5.00	7.68×10^{10}	8.20×10^{10}	2.36×10^9	2.55×10^9
10.00	1.68×10^{13}	1.64×10^{13}	7.24×10^{11}	7.16×10^{11}
25.00	1.00×10^{18}	8.34×10^{17}	6.97×10^{16}	5.87×10^{16}
50.00	1.78×10^{23}	1.26×10^{23}	1.85×10^{22}	1.32×10^{22}

[a]DOS: density of states, SOS: sum of states, and IL: inverse Laplace transform. All results in this table are calculated by MPW1K/MG3S using the inverse Laplace transform algorithm; a table with more energies and with a comparison to results obtained with the Beyer–Swinehart algorithm is given as Table S13. The energy E for this table is relative to zero-point energy of TS6 (which is 79.56 kcal/mol).

TS6 computed from multiple-structure quasi-harmonic-oscillator[87] (MS-QH) and MS-T partition functions at several energies; we discuss the results using the relative energy defined by

$$E^+ = E - V_a^{\ddagger G} \tag{38}$$

where $V_a^{\ddagger G}$ is the analog of V_a^{AG} when the energies are evaluated at a saddle point rather than at the maximum of the ground-state vibrationally adiabatic potential curve and E^+ is the rovibrational energy above the conventional TST threshold. The MS-T density of states for TS6 is plotted in Figure 1, and Figure 2 shows its ratio to the MS-QH DOS. For $E^+ = 0-0.75$ kcal/mol, this ratio increases rapidly from 1.00 to 1.21, for $E^+ > 0.75$ kcal/mol, the ratio gradually decreases, and for $E^+ > 8.42$ kcal/mol, DOS^{MS-T} is smaller than DOS^{MS-QH}. At a very high energy of $E^+ = 50$ kcal/mol, torsional anharmonicity makes the DOS of TS6 smaller than the one computed under harmonic-oscillator approximation by a factor of 0.7.

4.4. High-Pressure-Limit Rate Constants. The high-pressure MS-CVT/SCT-computed rate constants for R1–R8 at various temperatures are in the Supporting Information. Hydrogen abstraction reactions R2–R4 are endothermic; reaction R1 and hydrogen addition reactions R5–R8 are exothermic. Classical reaction energies (ΔV) for R1–R8 are shown in the Supporting Information. These high-pressure rate constants are fitted, and the fitting parameters for forward reactions are listed in Table 4. Those for reverse reactions are
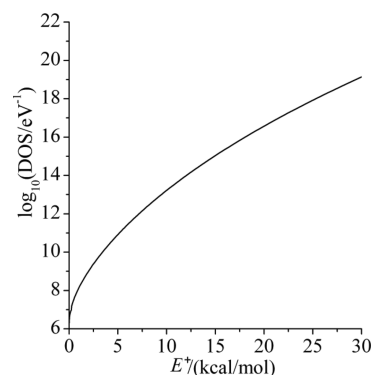

Figure 1. MS-T density of states (DOS) of TS6 at various energies. E^+ is the energy above the conventional TST threshold.
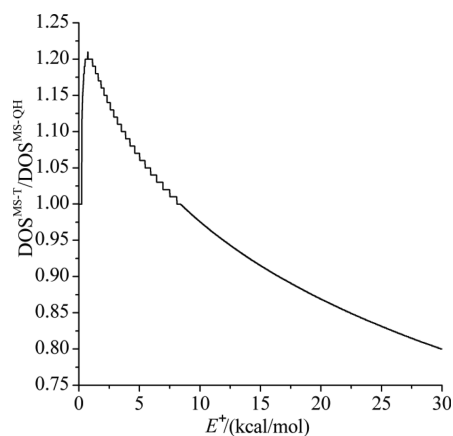

Figure 2. Ratios of density of states (DOS) computed from MS-T and MS-QH partition functions, DOS^{MS-T}/DOS^{MS-QH}, at various energies. E^+ is the energy above the conventional TST threshold.

Table 4. Fitting Parameters for MS-CVT/SCT High-Pressure-Limit Rate Constants at Various Temperatures of Forward Reactions R1–R9[a]

forward reactions	ln A	n	T_0 (K)	E (kcal/mol)
R1	−29.610	2.88	180.77	2.610
R2	−28.434	2.70	99.644	10.33
R3	−20.746	1.10	−5.228	15.97
R4	−25.997	1.82	−10.620	14.48
R5	−26.651	1.19	−39.943	6.425
R6	−25.821	1.24	−38.857	3.606
R7	−26.028	1.29	−39.693	4.103
R8	−26.736	1.50	−39.594	3.921
overall	−29.021	3.71	57.022	1.162
R9′	28.136	1.18	133.416	19.061

[a]Rate constants are in the unit of cm^3·molecule^{-1}·s^{-1}; overall (R1–R8) rate constants for forward reactions are fitted with exothermic formula.

listed in the Supporting Information. The rate constants of the dissociation of HT to benzene and methyl radical (R9′) are also included in this table. Temperature-dependent Arrhenius activation energies are computed using eq 7. Activation energies are shown in Tables S5 and S6.

Figure 3 shows the ratios of overall abstraction reaction rate constants ($k_1 + k_2 + k_3 + k_4$) to addition, i.e., methylcyclohexadienyl production, reaction rate constants ($k_5 + k_6 + k_7 + k_8$) at various temperatures, and at 0.1 bar, 1 bar, and the high-pressure
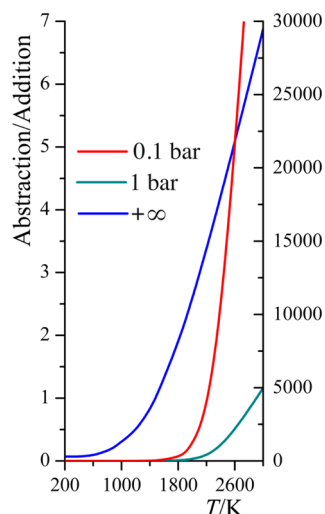
Figure 3. Ratios of the sum of abstraction reaction rate constants ($k_1 + k_2 + k_3 + k_4$) to the sum of addition (methylcyclohexadienyl production) reaction rate constants ($k_5 + k_6 + k_7 + k_8$) at various temperatures at 0.1 bar, 1 bar, and the high-pressure limit. The right ordinate scale is for 0.1 and 1 bar; the left ordinate scale is for the high-pressure limit.

Figure 4. MS-CVT/SCT rate constants (black line) and various experimental rate constants for R1 (hydrogen abstraction from the methyl group). MS-CVT/SCT rate constants for an abstraction reaction like R1 are independent of pressure.

Figure 5. Microcanonical variational transmission coefficients for reactions R5−R8 at various total rovibrational energies (kcal/mol).

limit. At high-pressure limit, as temperature increases, the ratio of abstraction to addition varies from 0.07 at 298 K to 6.88 at 3000 K. At lower temperatures (<1500 K), addition dominates abstraction; at 1500 K, abstraction and addition have the same contribution to the total reaction rate at the high-pressure limit (abstraction/addition = 1.04). At higher temperatures, hydrogen abstraction becomes important. Our computed abstraction/addition ratio is consistent with that of experimental work[4] using GC analysis that had concluded that at high-pressure limit the ratio of abstraction to addition reactions must be smaller than 0.17 at 298 K. At 298 K and 1 or 0.1 bar, ratios of abstraction to addition are essentially the same as those at high-pressure limit because of the negligible falloff effect at 298 K, though they might at first be different in the plot because they are plotted using different scales. (Details of falloff effect will be discussed in section 4.6.) At 1 and 0.1 bar, when the temperature is lower than 800 K, ratios of abstraction to addition are very close to the values at high-pressure limit because the falloff effects are not significant at these low temperatures. The falloff effects become more significant as temperature increases; thus, the rate constants for addition reactions are further decreased, which increases the ratio of abstraction to addition. At high temperatures, the ratios of abstraction to addition are significantly different at different pressures; at 3000 K, the ratios at 0.1 bar, 1 bar, and the high-pressure limit are respectively 4.9×10^4, 5.0×10^3, and 6.9.

Figure 4 shows MS-CVT/SCT high-pressure-limit rate constants and various experimentally measured rate constants for reaction R1 (hydrogen abstraction from the methyl group). Reactions R1−R4 are bimolecular reactions, and we consider gas-phase bimolecular reactions to be in the high-pressure plateau where collisions are efficient enough to maintain Boltzmann thermal equilibrium states. Our computed high-pressure-limit rate constants of the bimolecular reaction R1 agree very well with the measured rate constants.[6−8]

4.5. Microcanonical Rate Constants. Figure 5 shows a plot of the calculated microcanonical variational transmission coefficients $\Gamma^{\mu VT}(E)$ for reactions R5−R8; reverse and forward reactions have the same values of variational transmission coefficients (where reverse reactions correspond to $k_{-1}(E)$ in
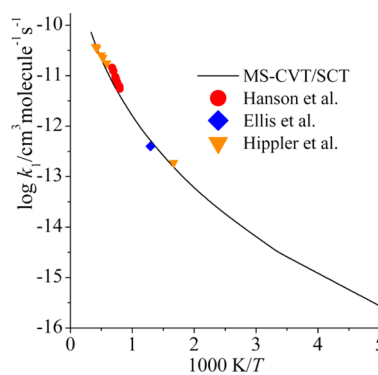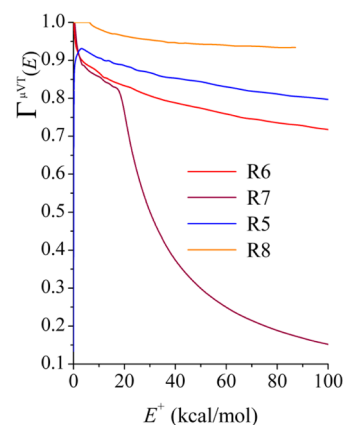
chemical activation mechanism) at various total rovibrational energies. The variational effects are important for computing microcanonical rate constants in all of these cases, especially for reverse reaction R7 at high energies and reverse reaction R5 at energies that are near the barrier, in which the variational transmission coefficients are significantly smaller than unity.

Figure 6 shows the microcanonical rate constants of reverse reaction of R6 computed by QRRK theory with s being the number of vibrational degrees of freedom (denoted as F), by QRRK theory with s being half of vibrational degrees of freedom, i.e., $F/2$, and by MS-μVT theory. Microcanonical rate constants computed by MS-μVT theory do not contain microcanonical tunneling correction; QRRK theory rate constants are calibrated by MS-CVT without canonical SCT tunneling. This figure is used to validate our calibrated QRRK method.

For falloff calculations, microcanonical rate constants computed by QRRK theory are calibrated by MS-CVT with canonical SCT tunneling corrections. One does not have to compute microcanonically tunneling-corrected MS-μVT rate constants; QRRK rate constants calibrated by high-pressure-limit MS-CVT with canonical tunneling are a more efficient and simpler approach than microcanonical MS-μVT/SCT.

Canonical VTST and microcanonical VTST are done in different ways: In canonical VTST, the generalized Gibbs free energy of activation is maximized; in microcanonical VTST, the number of states of the generalized transition state is minimized. Table 5 is only used to check if our computed MS-μVT
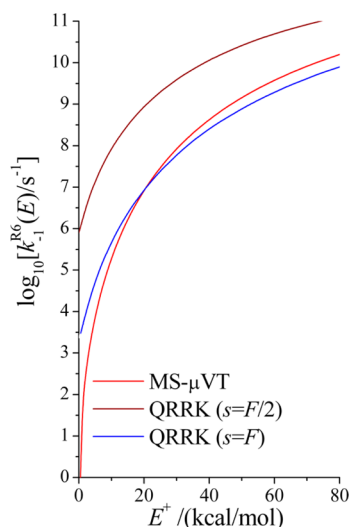
Figure 6. Microcanonical rate constants for reverse reaction of R6 computed by MS-μVT theory, by SS-QRRK theory with s being the number of vibrational degrees of freedom (denoted as F, which is 42 in the present case), and by SS-QRRK theory with $s = F/2$. SS-QRRK theory is calibrated by the high-pressure-limit MS-CVT rate constant without tunneling; the parameters A and E_0 are the same as those for $s = F$ and $F/2$ cases. Notice that although the validation (shown here) of SS-QRRK is done without tunneling, the parametrization of SS-QRRK used in the calculations of this paper for computing falloff does include tunneling as explained in the text.

microcanonical rate constants are in reasonable agreement with CVT values, and this is done by numerically integrating MS-μVT $k(E)$. The resulting difference between CVT and MS-μVT $k(T)$ is tiny. At medium-energy range (~10−50 kcal/mol), the microcanonical rate constants computed by QRRK with $s = F$ (calibrated by MS-CVT) matches very well with the computed $k^{\text{MS-}\mu\text{VT}}(E)$. Microcanonical rate constants at very high energy range do not contribute significantly in the canonically averaged rate constants because of negligible populations of reactant at these energies.

Table 5 shows canonical unimolecular rate constants for the reverse reaction of R6 computed by MS-CVT/SCT and MS-μVT/SCT. The canonical rate constants computed by these two approaches are in excellent agreement for the studied cases.

4.6. Pressure Dependence. The falloff effect of reaction Ri is characterized by the ratio of rate constant at pressure p to the high-pressure-limit rate constant, i.e., $k_{\text{stab}}(\text{R}i)/k_1(\text{R}i)$; the overall falloff for addition reactions (reactions R5−R8) is represented by the ratio $k_{\text{stab}}(\text{overall})/k_1(\text{overall})$, where "overall" means the summation from R5 to R8. The values of the QRRK parameters $A(T)$ and $E_0(T)$, determined as explained in section 2.3.1.1, are tabulated in Table S11. Figure 7 shows the falloff curves at
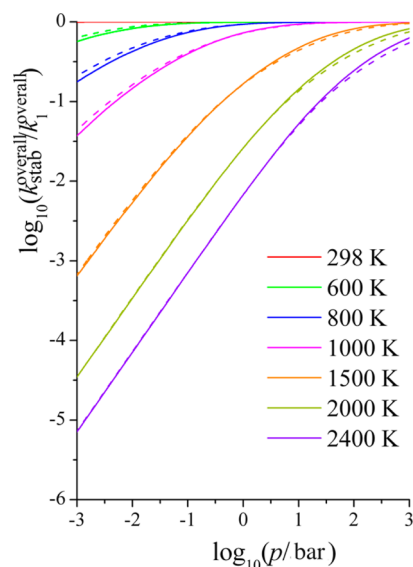

Figure 7. Falloff curves for overall addition reaction (sum of reactions R5−R8) computed by QRRK theory (dashed lines) and by MS-μVT theory (solid lines) at various pressures.

various temperatures (K) for overall addition reactions at various pressures (bar) computed by QRRK theory and by MS-μVT theory. (Pressures up to about 100 bar are important for combustion, and even higher pressures are shown to illustrate the approach to the high-pressure limit.) At all temperatures, the falloff curves predicted by QRRK theory and MS-μVT theory are in excellent agreement. This result is very encouraging and means that our way of doing QRRK calculations not only can provide an accurate description of falloff effects (compared with MS-μVT) but also is simple enough that the required input information is significantly small. This represents a breakthrough in using QRRK theory to predict falloff effects. Figure 8 plotted the falloff and dissociation curves (k_{benzene}/k_1) for reaction R5 at various pressures.

The advantage of the current version of QRRK theory for estimating falloff curves is that although the input data required is substantially simplified, the method is still able to give reasonable estimates for the falloff curves especially around ignition temperatures. Previous study[14] has shown that the differences between the simplified strong-collision model and the master equation approach are very small (~20% error for $CH_3 + C_2H_4$ addition reaction), and the extent of error is insensitive to the pressure. Jasper, Miller, and Klippenstein[88] have run classical trajectory calculations for methane colliding with a variety of bath gas molecules and concluded that Troe's approximation for computing the collision efficiency is capable of providing reasonably accurate predictions. Golden and co-workers[89]

Table 5. Canonical High-Pressure-Limit Unimolecular Rate Constants for the Reverse Reaction of R6 Computed by MS-CVT/SCT and MS-μVT/SCT at Various Temperatures

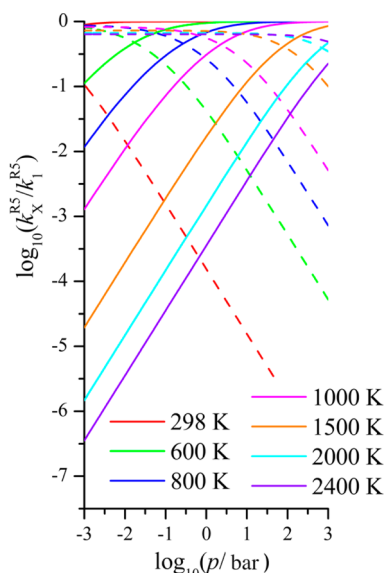| T (K)	$k^{\text{MS-CVT/SCT}}(T)$ (s^{-1})	$k^{\text{MS-}\mu\text{VT/SCT}}(T)$ (s^{-1})	T (K)	$k^{\text{MS-CVT/SCT}}(T)$ (s^{-1})	$k^{\text{MS-}\mu\text{VT/SCT}}(T)$ (s^{-1})
298.15	2.41×10^{-9}	2.20×10^{-9}	1000	1.06×10^{7}	1.05×10^{7}
300	3.27×10^{-9}	3.00×10^{-9}	1200	1.43×10^{8}	1.42×10^{8}
400	9.03×10^{-4}	8.92×10^{-4}	1400	9.21×10^{8}	9.21×10^{8}
500	1.98	1.91	1500	1.92×10^{9}	1.92×10^{9}
600	3.34×10^{2}	3.32×10^{2}	1800	1.09×10^{10}	1.09×10^{10}
800	2.15×10^{5}	2.14×10^{5}	2000	2.55×10^{10}	2.54×10^{10}
900	1.86×10^{6}	1.84×10^{6}	2400	9.15×10^{10}	9.10×10^{10}

Figure 8. Falloff curves (solid lines, X = stab) and dissociation curves (dashed lines, X = benzene) for reaction R5 computed by MS-μVT theory at various pressures (bar).

concluded that the classical RRK method with $s = C_V/R$ is adequate for predicting the unimolecular falloff to within a factor of 2 or 3 on the basis of the comparisons between classical RRK and RRKM theories for a wide range of dissociation reactions. The current approach also allows for analyzing the falloff effects for much more complex reactions with a large number of possible reaction channels.

Thus, for the purpose of efficiently estimating the falloff effects, the QRRK approach calibrated to MS-CVT/SCT (used here) is one reasonable choice. An alternative would be to use MS-μVT/SCT; however, the formulation of MS-μVT/SCT is significantly more complicated. Even MS-μVT without tunneling requires much more work than QRRK because of the number of states and density of states needed. In the present work, we use MS-μVT without tunneling to validate QRRK, and then we use QRRK calibrated to MS-CVT/SCT, which does include tunneling.

We found that the falloff effects are important at higher temperatures (>800 K) and negligible in lower temperature ranges. This observation is consistent with previous studies[14] for methyl radical recombination reactions and radical addition to unsaturated hydrocarbons.

The present article removes the empiricism in the treatment of the energy-dependent reaction rate constants, but it still uses a simplified treatment of the energy transfer collisions. Recent progress[90] in the treatment of energy transfer collisions could be combined with the approach used here to improve both aspects, but that is a separate issue and would increase the cost and computational effort considerably.

A limitation of this approach for multireaction pathways from the same excited intermediate is that it does not allow for fast depletion of energy levels by low-barrier paths that would otherwise have been available to contribute to the slower high-barrier pathways. Master equation methods would be able to model this phenomenon. In the current system, every channel has a distinct barrier; for barrierless reactions (such as radical–radical association reactions), other theoretical methodologies, e.g., variable reaction coordinate variational transition state

theory,[91] are needed for computing high-pressure-limit rate constants, which is out of the scope of the current work.

4.7. Comparison between Experimental and Computed Rate Constants. Our computed high-pressure-limit rate constant for the overall reaction (R1–R9) at 298 K is 4.87×10^{-14} cm^3 molecule^{-1} s^{-1}, which agrees very well with Robb's[3] experimental value of 4.0×10^{-14} cm^3 molecule^{-1} s^{-1}.

Our computed high-pressure-limit rate constant for summation of reactions R5–R8 at 298 K is 4.6×10^{-14} cm^3 molecule^{-1} s^{-1}. We showed in the previous section that the pressure falloff effects for reaction R5–R8 at 298 K are negligible; in particular, $\log_{10}[k_{stab}(R5-R8)/k_1(R5-R8)]$ ranges from -1.8×10^{-9} to -1.6×10^{-3} in the pressure range of 10^3-10^{-3} bar by MS-μVT theory. The experiments[4] by Sauer and Ward led to a high-pressure-limit rate constant for reactions R5–R8 at 298 K of 1.7×10^{-13} cm^3 molecule^{-1} s^{-1} (with a stated uncertainty of ±20%), which is about a factor of 3.6 larger than our computed high-pressure-limit value (4.6×10^{-14} cm^3 molecule^{-1} s^{-1}). They also concluded that within the experimental uncertainty there is no pressure dependence of the overall rate constants, and this conclusion is consistent with our falloff calculations.

Tsang[5] measured $k(R1-R4)/k_{methane}$ and $k_{benzene}/k_{methane}$, where $k_{methane}$ is the rate constant for H + CH$_4$ → H$_2$ + CH$_3$ at 950–1100 K. We recomputed his $k(R1-R4)$ and $k_{benzene}$ by using the modern experimental values for $k_{methane}$ reported by Sutherland et al.[92] The ratios of $k_{methane}$ reported by Sutherland et al. compared to to those used in Tsang's work are 0.65, 0.67, and 0.71 at 950, 1000, and 1100 K respectively; the final rate constants for $k(R1-R4)$ and $k(R9)$ measured by Tsang are multiplied by these three numbers at these temperatures in our comparison. The ratios of our computed $k(R1-R4)$ to the resulting experimental values at 950, 1000, and 1100 K are 0.96, 1.5, and 1.4 respectively, which is in excellent agreement. The ratios of the computed $k_{benzene}$ using 2 atm of Ar as bath gas to the experimental reported values in Tsang's work are 0.34, 0.37, and 0.46 at 950, 1000, and 1100 K, respectively, which is again in reasonable agreement for absolute rate constants for such a difficult problem, both experimentally and theoretically.

The experimentally determined rate constants of the bimolecular reaction R1 from Hippler et al.[6] are shown in Figure 4, which agree very well with our theoretically computed values.

The rate constant of reaction R1 at 773 K measured by Ellis[7] is $(4.0 \pm 0.8) \times 10^{-13}$ cm^3 molecule^{-1} s^{-1}; our computed rate constant of R1 at 773 K is 3.0×10^{-13} cm^3 molecule^{-1} s^{-1}, again showing good agreement. By using both experimental benzene yields and computer simulations, they estimated $k_{benzene} = (4.4 \pm 0.6) \times 10^{-13}$ cm^3 molecule^{-1} s^{-1}, at 773 K for a 500 Torr mixture of H$_2$, O$_2$, and N$_2$ as bath gas. (The amount of each gas varies in different experimental runs.) By using H$_2$ as bath gas, our computed $k_{benzene}$ at 773 K and 500 Torr is 7.2×10^{-14} cm^3 molecule^{-1} s^{-1}.

Hanson[8] measured the rate constant of bimolecular reaction R1 from 1256 to 1667 K. Figure 4 shows that our computed rate constant of R1 agrees very well with their experimental values.

4.8. Branching Fractions. Reaction R6 has the lowest barrier among all the reactions, whereas reaction R3 has the highest. Because hydrogen addition reactions have smaller barriers than hydrogen abstraction reactions and because the branching fractions for radical addition at various positions are not available experimentally, their calculation in the present study can be especially useful in guiding combustion mechanisms. The branching fraction of reaction Ri at temperature T and pressure p is computed as the ratio of the rate

constant of Ri (with the reactions labeled as in Scheme 1) to the overall rate constant (R1–R9) at temperature T and pressure p. Branching fractions computed for reactions R1, R3, and R6–R8, which are major contributors to the overall reactions, are plotted in Figure 9: the solid curves are MS-CVT results in the high-pressure limit; the dashed curves are predictions by MS-μVT at 1.0 bar. Additional branching fractions are plotted in Figure S1.
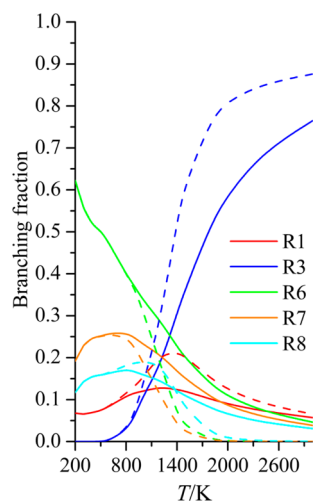

Figure 9. Branching fractions of reactions R1, R3, and R6–R8 as functions of temperature as predicted by MS-CVT/SCT high-pressure-limit rate constants (solid lines) and by MS-μVT theory at 1.0 bar (dashed lines). The branching fraction of reaction Ri is computed as the ratio of rate constant of Ri to the overall rate constant (R1–R9).

At the high-pressure limit and at temperatures lower than 1000 K, hydrogen addition reactions R6 and R7 are the dominant reactions; this is consistent with what we show in Figure 3. The sum of the branching fractions of R6 and R7 gradually decreases from 81% at 200 K to 57% at 1000 K and to 8.5% at 3000 K. The branching fraction of the hydrogen abstraction R3 (hydrogen abstraction from the meta position of the aromatic ring) increases from 1.6×10^{-10} % at 200 K to 6.0% at 900 K and to 77% at 3000 K.

At 1.0 bar, the branching fractions of R6 and R7 decrease more rapidly from 800 K than the ones at high-pressure limit. The maximum of the branching fraction of reaction R1 at the high-pressure limit is 13% at 1200 K. At a pressure of 1.0 bar, from 600 K on, the branching fraction of R1 rises more rapidly than at the high-pressure limit, and it reaches its maximum of 20.4% at 1400 K, then decreases more slowly than the one at high-pressure limit. Branching fractions of reaction R3 increase more rapidly at 1.0 bar than the ones in the high-pressure limit; at 3000 K, R3's branching fraction at 1.0 bar is 10.4% higher than the one at the high-pressure limit.

Figure 10 shows the predicted branching fractions for reaction R3 (solid lines) and R6 (dashed lines) as functions of pressure (bar) at 800, 1400, and 2000 K. Falloff effects are negligible at low temperatures (<800 K); therefore, the pressure dependence of branching fractions at low temperatures is negligible. At high temperatures (T > 2000 K), although the falloff effects are very important, the overall reaction rate constants are dominated by abstraction reactions and not by addition reactions, and the branching ratios of addition reactions are negligible. The branching fraction of abstraction reaction R6, which is the dominate reaction at high temperatures, is not very sensitive to
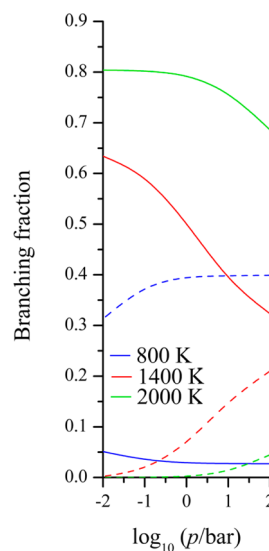

Figure 10. Branching fractions of reactions R3 (solid lines) and R6 (dashed lines) as functions of pressure (bar) as predicted by MS-μVT theory at 800, 1400, and 2000 K.

the variation of pressures. (It decreases from 80.4% to 68.6% as pressure increases from 0.01 to 100 bar at 2000 K.) At 1400 K, branching fractions of both R3 and R6 are quite sensitive to the change of pressures: From 0.01 to 100 bar, the branching fraction of R3 decreases by a factor of 2, whereas the branching fraction of R6 increases significantly by a factor of 102.

5. SUMMARY AND CONCLUSIONS

In the current work, high-pressure-limit rate constants and pressure-dependent rate constants have been calculated for both hydrogen abstraction and addition reactions of toluene reacting with hydrogen radical. Our computed rate constants agree very well with experimentally measured rate constants. We have compared several model chemistries for the energetics of toluene + H reactions, and possible sources of errors are analyzed. Multiple-structure and torsional anharmonicity effects on the density of rovibrational states have been discussed. To model the pressure falloff effects on the hydrogen addition reactions, a simple but reasonable and efficient model is proposed, which is based on chemical activation theory, modified strong-collision theory, and our MS-CVT/SCT high-pressure-limit rate constants. In the chemical activation mechanism, we implemented two approaches to compute the microcanonical rate constant: quantum RRK theory and microcanonical variational transition state theory (MS-μVT). This allows the radical association to be treated conveniently at a level of dynamical theory consistent with the treatment of bimolecular atom transfer reactions. Our version of QRRK theory agrees excellently with MS-μVT theory in all temperature ranges.

We found that the variational effect is important in computing the microcanonical rate constants; thus, it is necessary to include such effects in computing $k(E)$. We have shown that the pressure falloff effects for the addition reactions at 298 K are negligible, which is consistent with our computed overall high-pressure-limit rate constant agreeing very well with the experimentally measured rate constant at 298 K and 6.8 Torr. Our computed high-pressure-limit rate constants for the bimolecular reaction R1 agree very well with experimentally measured rate constants at various temperatures. The ratios of abstraction to addition reactions at the high-pressure limit at various temperatures have

also been calculated, and these ratios are experimentally hard to measure. The pressure dependences of addition reactions (R5−R8) are predicted to be more important at high temperatures (>800 K) than at low temperature ranges.

Branching fractions for the H reaction with toluene are both temperature- and pressure-dependent. We showed that the hydrogen abstraction from *meta*-H of toluene (reaction R3) is the dominant reaction at high temperature (>2000 K); the branching fraction of the hydrogen addition at ortho position of the aromatic ring (reaction R6) is larger than 50% at low temperatures (<500 K). The contribution of reaction R3 to the overall rate constant increases more rapidly at 1.0 bar than at the high-pressure limit; the branching fraction of reaction R6 deceases more rapidly at 1.0 bar than at the high-pressure limit. The behaviors of branching ratio curves are not the same at different pressures.

■ ASSOCIATED CONTENT

Ⓢ Supporting Information

The Supporting Information is available free of charge on the ACS Publications website at DOI: 10.1021/jacs.5b11938.

> Testing of electronic structure methods and selection of an electronic structure method to use for direct dynamics, computational details of electronic structure calculations and the direct dynamics calculations, Cartesian coordinates of optimized geometries, computed MS-CVT/SCT rate constants at various temperatures, classical reaction energies for R1−R8, fitting parameters for reverse rate constants, activation energies, Arrhenius pre-exponential factors A, and vibrational frequencies. (PDF)

■ AUTHOR INFORMATION

Corresponding Author
*E-mail: truhlar@umn.edu

Present Address
J.Z.: Gaussian, Inc. 340 Quinnipiac St. Bldg. 40, Wallingford, CT 06492

Notes
The authors declare no competing financial interest.

■ ACKNOWLEDGMENTS

■ REFERENCES

(1) Battin-Leclerc, F. *Prog. Energy Combust. Sci.* **2008**, *34*, 440.
(2) Ribaucour, M. A.; Roubaud, A.; Minetti, R.; Sochet, L. R. *Proc. Combust. Inst.* **2000**, *28*, 1701.
(3) Allen, P. E. M.; Melville, H. W.; Robb, J. C. *Proc. R. Soc. London, Ser. A* **1953**, *218*, 311.
(4) Sauer, M. C.; Ward, B. *J. Phys. Chem.* **1967**, *71*, 3971.
(5) Robaugh, D.; Tsang, W. *J. Phys. Chem.* **1986**, *90*, 4159.
(6) Hippler, H.; Reihs, C.; Troe, J. *Z. Phys. Chem. (Muenchen, Ger.)* **1990**, *167*, 1.
(7) Ellis, C.; Scott, M. S.; Walker, R. W. *Combust. Flame* **2003**, *132*, 291.
(8) Oehlschlaeger, A. M.; Davidson, D. F.; Hanson, R. K. *J. Phys. Chem. A* **2006**, *110*, 9867.
(9) Liu, Y.-P.; Lu, D.-h.; Gonzàlez-Lafont, A.; Truhlar, D. G.; Garrett, B. C. *J. Am. Chem. Soc.* **1993**, *115*, 7806.
(10) Fernández-Ramos, A.; Miller, J. A.; Klippenstein, S. J.; Truhlar, D. G. *Chem. Rev.* **2006**, *106*, 4518.
(11) Barker, J. R. *Int. J. Chem. Kinet.* **2009**, *41*, 748.
(12) Glowacki, D. R.; Liang, C.-H.; Morley, C.; Pilling, M. J.; Robertson, S. H. *J. Phys. Chem. A* **2012**, *116*, 9545.
(13) Klippenstein, S. J.; Pande, V.; Truhlar, D. G. *J. Am. Chem. Soc.* **2014**, *136*, 528.
(14) Dean, A. M. *J. Phys. Chem.* **1985**, *89*, 4600.
(15) Yu, T.; Zheng, J.; Truhlar, D. G. *Chem. Sci.* **2011**, *2*, 2199.
(16) Garrett, B. C.; Truhlar, D. G. *J. J. Chem. Phys.* **1979**, *70*, 1593.
(17) Truhlar, D. G.; Garrett, B. C. *Acc. Chem. Res.* **1980**, *13*, 440.
(18) Holbrook, K. A.; Pilling, M. J.; Robertson, S. H. In *Unimolecular Reactions*; John Wiley & Sons: New York, 1996.
(19) Tardy, D. J.; Rabinovitch, B. S. *Chem. Rev.* **1977**, *77*, 369.
(20) Kassel, L. S. *J. Phys. Chem.* **1927**, *32*, 225.
(21) Kassel, L. S. *Kinetics of Homogenous Gas Reactions*; Chemical Catalog Co.: New York, 1932.
(22) Troe, J. *J. Phys. Chem.* **1979**, *83*, 114.
(23) Troe, J. *J. Chem. Phys.* **1977**, *66*, 4745.
(24) Troe, J. *J. Chem. Phys.* **1977**, *66*, 4758.
(25) Lefort, B.; Tsang, W. *Combust. Flame* **2011**, *158*, 657.
(26) Seal, P.; Papajak, E.; Truhlar, D. G. *J. Phys. Chem. Lett.* **2012**, *3*, 264.
(27) Xu, X.; Yu, T.; Papajak, E.; Truhlar, D. G. *J. Phys. Chem. A* **2012**, *116*, 10480.
(28) Alecu, I. M.; Zheng, J.; Papajak, E.; Yu, T.; Truhlar, D. G. *J. Phys. Chem. A* **2012**, *116*, 12206.
(29) Xu, X.; Papajak, E.; Zheng, J.; Truhlar, D. G. *Phys. Chem. Chem. Phys.* **2012**, *14*, 4204.
(30) Yu, T.; Zheng, J.; Truhlar, D. G. *J. Phys. Chem. A* **2012**, *116*, 297.
(31) Truhlar, D. G.; Isaacson, A. D.; Garrett, B. C. In *Theory of Chemical Reaction Dynamics*; Baer, M., Ed.; CRC Press: Boca Raton, FL, 1985; pp 65−137.
(32) Fernandez-Ramos, A.; Ellingson, B. A.; Garrett, B. C.; Truhlar, D. G. *Rev. Comp. Chem.* **2007**, *23*, 125.
(33) Zheng, J.; Truhlar, D. G. *J. Chem. Theory Comput.* **2013**, *9*, 2875.
(34) Liu, Y. P.; Lynch, G. C.; Truong, T. N.; Lu, D.-H.; Truhlar, D. G.; Garrett, B. C. *J. Am. Chem. Soc.* **1993**, *115*, 2408.
(35) Alecu, I. M.; Zheng, J.; Zhao, Y.; Truhlar, D. G. *J. Chem. Theory Comput.* **2010**, *6*, 2872.
(36) Zheng, J.; Meana-Pañeda, R.; Truhlar, D. G. *J. Am. Chem. Soc.* **2014**, *136*, 5150.
(37) Zheng, J.; Seal, P.; Truhlar, D. G. *Chem. Sci.* **2013**, *4*, 200.
(38) Bao, J. L.; Meana-Pañeda, R.; Truhlar, D. G. *Chem. Sci.* **2015**, *6*, 5866.
(39) Bao, J. L.; Seal, P.; Truhlar, D. G. *Phys. Chem. Chem. Phys.* **2015**, *17*, 15928.
(40) Bao, J. L.; Sripa, P.; Truhlar, D. G. *Phys. Chem. Chem. Phys.* **2016**, *18*, 1032.
(41) Zheng, J.; Yu, T.; Papajak, E.; Alecu, I. M.; Mielke, S. L.; Truhlar, D. G. *Phys. Chem. Chem. Phys.* **2011**, *13*, 10885.
(42) Zheng, J.; Truhlar, D. G. *J. Chem. Theory Comput.* **2013**, *9*, 1356.
(43) Zheng, J.; Mielke, S. L.; Clarkson, K. L.; Truhlar, D. G. *Comput. Phys. Commun.* **2012**, *183*, 1803.
(44) Zheng, J.; Meana-Pañeda, R.; Truhlar, D. G. *Comput. Phys. Commun.* **2013**, *184*, 2032.
(45) Rauhut, G.; Pulay, P. *J. Phys. Chem.* **1995**, *99*, 3093.
(46) Alecu, I. M.; Zheng, J.; Zhao, Y.; Truhlar, D. G. *J. Chem. Theory Comput.* **2010**, *6*, 2872.
(47) Bloino, J.; Biczysko, M.; Barone, V. *J. Chem. Theory Comput.* **2012**, *8*, 1015.
(48) Kuhler, K. M.; Truhlar, D. G.; Isaacson, A. D. *J. Chem. Phys.* **1996**, *104*, 4664.
(49) Nielsen, H. H. *Encycl. Phys.* **1959**, *7/37/1*, 173.
(50) Zhang, Q.; Day, P. N.; Truhlar, D. G. *J. Chem. Phys.* **1993**, *98*, 4948.
(51) Chuang, Y.-Y.; Truhlar, D. G. *J. Chem. Phys.* **1997**, *107*, 83.
(52) Fernández-Ramos, A.; Ellingson, B. A.; Meana-Pañeda, R.; Marques, J. M. C.; Truhlar, D. G. *Theor. Chem. Acc.* **2007**, *118*, 813.
(53) Zheng, J.; Truhlar, D. G. *Phys. Chem. Chem. Phys.* **2010**, *12*, 7782.
(54) Zheng, J.; Truhlar, D. G. *Faraday Discuss.* **2012**, *157*, 59.

(55) Tolman, R. C. *J. Am. Chem. Soc.* **1920**, *42*, 2506.

(56) Truhlar, D. G. *J. Chem. Educ.* **1978**, *55*, 309.

(57) Warnatz, J. *Combust. Sci. Technol.* **1983**, *34*, 177.

(58) Eggers, D. F., Jr.; Gregory, N. W.; Halsey, G. D.; Rabinovitch, B. S. *Physical Chemistry*; Wiley: New York, 1964; p 458.

(59) Schranz, H. W.; Nordholm, S.; Hamer, N. D. *Int. J. Chem. Kinet.* **1982**, *14*, 543.

(60) Chang, A. Y.; Bozzelli, J. W.; Dean, A. M. *Z. Phys. Chem.* **2000**, *214*, 1533.

(61) Westmoreland, P. R.; Howard, J. B.; Longwell, J. P.; Dean, A. M. *AIChE J.* **1986**, *32*, 1971.

(62) Bozzelli, J. W.; Dean, A. M. *J. Phys. Chem.* **1990**, *94*, 3313.

(63) Bozzelli, J. W.; Chang, A. Y.; Dean, A. M. *Int. J. Chem. Kinet.* **1997**, *29*, 161.

(64) Marcus, R. A.; Rice, O. K. *J. Phys. Chem.* **1951**, *55*, 894.

(65) Marcus, R. A. *J. Chem. Phys.* **1952**, *20*, 359.

(66) Rosenstock, H. M.; Wallenstein, M. B.; Wahrhaftig, A. L.; Eyring, H. *Proc. Natl. Acad. Sci. U. S. A.* **1952**, *38*, 667.

(67) Magee, J. L. *Proc. Natl. Acad. Sci. U. S. A.* **1952**, *38*, 764.

(68) Garrett, B. C.; Truhlar, D. G.; Grev, R. S.; Magnuson, A. W. *J. Phys. Chem.* **1980**, *84*, 1730.

(69) Sheng, C. Y.; Bozzelli, J. W.; Dean, A. M.; Chang, A. Y. *J. Phys. Chem. A* **2002**, *106*, 7276.

(70) Carstensen, H.-H.; Naik, C. V.; Dean, A. M. *J. Phys. Chem. A* **2005**, *109*, 2264.

(71) Hirschfelder, J. O.; Curtiss, C. F.; Bird, R. B. In *Molecular Theory of Gases and Liquids*; Wiley and Sons: London, 1967.

(72) Reid, R. C.; Prausnitz, J. M.; Sherwood, T. K. In *The Properties of Gases and Liquids*; McGraw-Hill: New York, 1977.

(73) Forst, W. In *Theory of Unimolecular Reactions*; Academic Press: New York, 1973.

(74) Zheng, J.; Zhang, S.; Corchado, J. C.; Chuang, Y. Y.; Coitino, E. L.; Ellingson, B. A.; Truhlar, D. G. *GAUSSRATE*, version 2009-A; University of Minnesota: Minneapolis, MN, 2010.

(75) Zheng, J.; Zhang, S.; Lynch, B. J.; Corchado, J. C.; Chuang, Y.-Y.; Fast, P. L.; Hu, W.-P.; Liu, Y.-P.; Lynch, G. C.; Nguyen, K. A.; Jackels, C. F.; Fernandez Ramos, A.; Ellingson, B. A.; Melissas, V. S.; Villà, J.; Rossi, I.; Coitiño, E. L.; Pu, J.; Albu, T. V.; Ratkiewicz, A.; Steckler, R.; Garrett, B. C.; Isaacson, A. D.; Truhlar, D. G. *POLYRATE*, version 2010-A; University of Minnesota: Minneapolis, MN, 2010.

(76) Zheng, J.; Mielke, S. L.; Clarkson, K. L.; Meana-Pañeda, R.; Truhlar, D. G. *MSTor*, version 2013; University of Minnesota: Minneapolis, MN, 2013.

(77) Frisch, M. J.; Trucks, G. W.; Schlegel, H. B.; Scuseria, G. E.; Robb, M. A.; Cheeseman, J. R.; Scalmani, G.; Barone, V.; Mennucci, B.; Petersson, G. A.; Nakatsuji, H.; Caricato, M.; Li, X.; Hratchian, H. P.; Izmaylov, A. F.; Bloino, J.; Zheng, G.; Sonnenberg, J. L.; Hada, M.; Ehara, M.; Toyota, K.; Fukuda, R.; Hasegawa, J.; Ishida, M.; Nakajima, T.; Honda, Y.; Kitao, O.; Nakai, H.; Vreven, T.; Montgomery, J. A., Jr.; Peralta, J. E.; Ogliaro, F.; Bearpark, M.; Heyd, J. J.; Brothers, E.; Kudin, K. N.; Staroverov, V. N.; Kobayashi, R.; Normand, J.; Raghavachari, K.; Rendell, A.; Burant, J. C.; Iyengar, S. S.; Tomasi, J.; Cossi, M.; Rega, N.; Millam, J. M.; Klene, M.; Knox, J. E.; Cross, J. B.; Bakken, V.; Adamo, C.; Jaramillo, J.; Gomperts, R.; Stratmann, R. E.; Yazyev, O.; Austin, A. J.; Cammi, R.; Pomelli, C.; Ochterski, J. W.; Martin, R. L.; Morokuma, K.; Zakrzewski, V. G.; Voth, G. A.; Salvador, P.; Dannenberg, J. J.; Dapprich, S.; Daniels, A. D.; Farkas, O.; Foresman, J. B.; Ortiz, J. V.; Cioslowski, J.; Fox, D. J. *Gaussian 09*, revision x.x; Gaussian, Inc.: Wallingford, CT, 2009.

(78) Zhao, Y.; Peverati, R.; Yang, K.; He, X.; Yu, H.; Truhlar, D. G. *MN-GFM*, version 6.6 (computer program module); University of Minnesota; Minneapolis, MN, 2015.

(79) Hippler, H.; Troe, J.; Wendelken, H. J. *J. Chem. Phys.* **1983**, *78*, 6709.

(80) Eng, R. A.; Gebert, A.; Goos, E.; Hippler, H.; Kachiani, C. *Phys. Chem. Chem. Phys.* **2002**, *4*, 3989.

(81) Rahman, A. *Phys. Rev.* **1964**, *136*, A405.

(82) Adler, T. B.; Knizia, G.; Werner, H. J. *J. Chem. Phys.* **2007**, *127*, 221106.

(83) Knizia, G.; Adler, T. B.; Werner, H. J. *J. Chem. Phys.* **2009**, *130*, 054104.

(84) Papajak, E.; Truhlar, D. G. *J. Chem. Phys.* **2012**, *137*, 064110.

(85) Lynch, B. J.; Fast, P. L.; Harris, M.; Truhlar, D. G. *J. Phys. Chem. A* **2000**, *104*, 4811.

(86) Lynch, B. J.; Zhao, Y.; Truhlar, D. G. *J. Phys. Chem. A* **2003**, *107*, 1384.

(87) Zheng, J.; Yu, T.; Papajak, E.; Alecu, I. M.; Mielke, S. L.; Truhlar, D. G. *Phys. Chem. Chem. Phys.* **2011**, *13*, 10885.

(88) Jasper, A. W.; Miller, J. A.; Klippenstein, S. J. *J. Phys. Chem. A* **2013**, *117*, 12243.

(89) Golden, D. M.; Solly, R. K.; Benzon, S. W. *J. Phys. Chem.* **1971**, *75*, 1333.

(90) Jasper, A. W.; Pelzer, K. M.; Miller, J. A.; Kamarchik, E.; Harding, L. B.; Klippenstein, S. J. *Science* **2014**, *346*, 1212.

(91) (a) Zheng, J.; Zhang, S.; Truhlar, D. G. *J. Phys. Chem. A* **2008**, *112*, 11509. (b) Georgievskii, Y.; Klippenstein, S. J. *J. Chem. Phys.* **2003**, *118*, 5442. (c) Georgievskii, Y.; Klippenstein, S. J. *J. Phys. Chem. A* **2003**, *107*, 9776. (d) Truhlar, D. G.; Garrett, B. C.; Klippenstein, S. J. *J. Phys. Chem.* **1996**, *100*, 12771. (e) Klippenstein, S. J. *J. Chem. Phys.* **1991**, *94*, 6469.

(92) Sutherland, J. W.; Su, M.-C.; Michael, J. V. *Int. J. Chem. Kinet.* **2001**, *33*, 669.